The Astrophysical Journal, 713:1167–1173, 2010 April 20 doi:10.1088/0004-637X/713/2/1167

LOWER BOUNDS ON PHOTOMETRIC REDSHIFT ERRORS FROM TYPE Ia SUPERNOVA TEMPLATES

S. Asztalos[1], S. Nikolaev[2], W. de Vries[2], S. Olivier[2], K. Cook[2], and L. Wang[3]
[1] XIA, LLC, Hayward, CA 94554, USA
[2] Lawrence Livermore National Laboratory, Livermore, CA 94551, USA
[3] Texas A&M, College Station, TX 77843, USA
Received 2009 October 2; accepted 2010 March 3; published 2010 March 31

ABSTRACT

Cosmology with Type Ia supernova heretofore has required extensive spectroscopic follow-up to establish an accurate redshift. Though this resource-intensive approach is tolerable at the present discovery rate, the next generation of ground-based all-sky survey instruments will render it unsustainable. Photometry-based redshift determination may be a viable alternative, though the technique introduces non-negligible errors that ultimately degrade the ability to discriminate between competing cosmologies. We present a strictly template-based photometric redshift estimator and compute redshift reconstruction errors in the presence of statistical errors. Under highly degraded photometric conditions corresponding to a statistical error σ of 0.5, the residual redshift error is found to be 0.236 when assuming a nightly observing cadence and a single Large Synoptic Science Telescope (LSST) *u*-band filter. Utilizing all six LSST bandpass filters reduces the residual redshift error to 9.1×10^{-3}. Assuming a more optimistic statistical error σ of 0.05, we derive residual redshift errors of 4.2×10^{-4}, 5.2×10^{-4}, 9.2×10^{-4}, and 1.8×10^{-3} for observations occuring nightly, every 5th, 20th and 45th night, respectively, in each of the six LSST bandpass filters. Adopting an observing cadence in which photometry is acquired with all six filters every 5th night and a realistic supernova distribution, binned redshift errors are combined with photometric errors with a σ of 0.17 and systematic errors with a $\sigma \sim 0.003$ to derive joint errors (σ_w, $\sigma_{w'}$) of (0.012, 0.066), respectively, in (w,w') with 68% confidence using Fisher matrix formalism. Though highly idealized in the present context, the methodology is nonetheless quite relevant for the next generation of ground-based all-sky surveys.

Key words: distance scale – methods: numerical

Online-only material: color figures

1. INTRODUCTION

Accumulating evidence for an accelerating universe (Riess et al. 1998; Perlmutter et al. 1999; Astier et al. 2006; Wood-Vasey et al. 2007) is premised on the photometry of several hundred Type Ia supernovae whose redshifts were exquisitely determined through lengthy spectroscopic follow-up. At the current Type Ia supernova discovery rate, this situation remains manageable and spectroscopic follow-up continues to be the norm. Nonetheless, we are embarking on an era where ground-based survey telescopes[4,5,6,7] may discover a million or more Type Ia supernovae per year of operation. This fantastic rate precludes spectroscopic follow up on all but the smallest fraction of supernovae.

Errors from spectroscopically determined redshifts (± 0.001) are typically much smaller than errors associated with other parameters (e.g., stretch and magnitude) used in constructing Hubble diagrams and are justifiably neglected. However, spectroscopically acquired redshifts typically require hours of dedicated time on large aperture follow-up telescopes. As future survey instruments may discover thousands of Type Ia supernovae every night, a different method for ascertaining redshifts certainly must be adopted. By contrast, photometrically acquired redshifts are constructed directly from the photometry. Unfortunately, photometric redshift reconstruction is imperfect by introducing non-negligible redshift errors that must be accounted for in subsequent analyses.

Serendipitously, both of the long-standing photometric redshift techniques developed for galactic astronomy can be brought to bear on assessing the photometric redshifts of Type Ia supernovae. As the field of galactic redshift determination matured, two competing techniques have emerged. The first technique is based on empirical fits derived from a galactic training set having well-established redshifts (see, e.g., Connolly et al. 1995). Recently, an empirical photometric estimator has been derived and applied to Type Ia supernovae (Wang 2007). With this technique, magnitudes derived from fluxes in the *grz* bands are linearly combined to give a first-order redshift estimate. An improved redshift estimate is obtained by adding a stretch-like correction involving a ratio of the *i* band fluxes at peak and at 15 days in the supernova rest frame. The coefficients are derived from a Supernova Legacy Survey (SNLS) training set of 40 Type Ia supernovae. A dispersion ranging 0.031–0.050 is reported depending on the size of the training set. These comparatively large numbers are attributed to the photometric quality of the SNLS data and minimal statistics. In a follow up paper (Wang et al. 2007), it was shown that a dispersion of 0.005 may be achievable from supernovae with a signal-to-noise ratio (S/N) > 25, albeit supernovae that are temporally well-sampled and free of obscuration from dust.

The second technique involves broadband photometry acquired over multiple bands, which is compared to predictions from galaxy spectral energy distributions to determine the redshift (Loh & Spillar 1986, recently improved on by Bolzonella & Pelló 2000). The photometric error from either approach can be of order ± 0.1, which is generally unacceptable for the study of individual galaxies or galaxy clusters, though is less problematic when performing statistical analyses of large

[4] http://msowww.anu.edu.au/skymapper/
[5] http://pan-starrs.ifa.hawaii.edu/public/
[6] http://www.lsst.org/lsst
[7] http://www.darkenergysurvey.org/

data sets. In this paper we adopt this latter approach to obtain photometric redshifts from template fitting, obviating the need for an empirical model. However, a faithful Type Ia template is required. The requirement of a faithful supernova template is non-trivial since no two supernovae have identical spectra, the spectra evolve with time and further exhibit variation in luminosity. Further, Type Ia supernovae have no Hydrogen features in their spectra and hence lack the Lyman-break used for determining galactic redshifts, though they are rich with other spectral features. In practice, temporal variation allows for an independent redshift determination at each epoch which are combined to jointly constrain the redshift.

The redshift error which results when the template approach is applied to Type Ia supernovae is the main objective of this paper. In Section 2, we describe the redshift error estimation methodology based on an archetypal Type Ia supernova template set. In Section 3, we present results based solely on statistical error, then extend them to include systematic error derived from a distinct template set. From these combined statistical and systematic errors, we derive in Section 4 error ellipses in the (w,w') plane based on a realistic supernova distribution and idealized cadence. We conclude in Section 5 with a discussion of the implications of our work and discuss possible future extensions.

2. METHODOLOGY

The template fitting method starts with a Type Ia supernova template set generated in the supernova rest frame. Modifications required to transform rest-frame fluxes into redshifted magnitudes are then applied (this modified set is henceforth referred to as the model set). The light curve of a supernova whose redshift is to be determined (the reference supernova) is then compared to light curves from the model set over a suitable redshift interval. The redshift of the light curve from the model set that most closely matches the light curve of the reference supernova (using a χ^2 figure of merit) is assigned to the latter.

Here we adopt Type Ia branch normal templates (Nugent et al. 2002) for our studies. These templates span the temporal range from −16 day prior to +70 days after peak V magnitude for a total of 87 epochs. The wavelength coverage is 1000–25000 Å binned into 2401 10 Å intervals. This set of 87 spectra constitutes the rest-frame template set. There are four operations that must be applied to this template set to generate the model set (representing supernovae spectra at various redshifts in an expanding universe). The first two each involves a reduction in the flux by a factor of $(1+z)$, where z runs from 0 to 1.0 in redshift intervals of 0.001, to account for time dilation and cosmological expansion (photon redshift; Weinberg 1972, p. 688). The third involves stretching the wavelength by $(1 + z)$. Each of these first three corrections can be applied either to the spectra or the inverse operation to the bandpass filters—the latter approach is chosen here for computational convenience. The fourth and final correction is a time dilation factor of $(1+z)$ applied to each epoch (Goldhaber et al. 1996).

The next step of the procedure requires specifying the bandpass filters. Two factors of $(1 + z)$ were applied to the Large Synoptic Science Telescope (LSST) bandpasses (Olivier et al. 2008), which incorporate sky and filter transmission and CCD efficiency. Bandpass fluxes were derived by convolving the modified $ugrizy$ LSST filters with the template set, after calibration using a Johnson B-band filter. Specifically, the Johnson B filter was convolved with the Nugent template at time of maximum light. The correction required to make the resulting B passband magnitude equal to −19.3 (Hillebrandt & Niemeyer 2000) was then applied to all subsequent data. The daily interval between successive epochs in the supernova rest frame is replaced by a separation of $(1 + z)$ days in the frame of the observer. The end result of this exercise is the creation of 1001 light curve files, each containing the magnitudes for all 87 (time dilated) epochs in all six filters. This collection comprises the model set. A key aspect of our method involves the conversion of magnitudes into colors. As is well known, the relationship between luminosity and flux requires knowledge of the luminosity distance, with the latter depending on the cosmological model. As will be made more explicit below, conversion from bandpass to color magnitudes permits cancellation of the (unknown) luminosity distance. The results are therefore independent of cosmological model, though are limited by the approximation that the peak luminosity of a Type Ia supernova is fixed at −19.3. Each panel in Figure 1 shows the evolution of five distinct LSST colors derived by applying the four operations described above to the Nugent template set. Each color is shown as a function of redshift for three well-separated epochs. Over the epoch range shown, the $g-r$ color exhibits nearly monotonic behavior and would be the most effective of the five colors over the depicted redshift interval in estimating redshifts. The actual reconstruction efficiency will be considerably more nuanced when multiple colors, multiple epochs, and measurement noise are involved, as we shall see below.

We now proceed to define a measure of goodness-of-fit $\chi^2(z)$ for the $u-g$ color as

$$\chi^2(z) = \sum_{z'}((u(z) - g(z)) - (u(z') - g(z')))^2. \qquad (1)$$

In this expression, $u(z)$ and $g(z)$ represent sums of magnitudes obtained by convolving rest-frame spectra over epochs of interest with modified u and g bandpasses, respectively. The sums $u(z')$ and $g(z')$ are defined similarly for the model set. This procedure is generalized in an obvious manner to include the five colors ($u-g$, $g-r$, $r-i$, $i-z$, and $z-y$) that can be constructed from the six LSST bandpasses. Note that Equation (1) makes explicit how luminosity distances cancel if one chooses to work with color magnitudes. The χ^2 expression described by Equation (1) is actually a 1001 element array, each element of the array containing one value for a given combination of (z, z'). The full array is generated by fixing z and varying z' over the interval $0 < z' < 1$ in increments of 0.001. The minimum value of χ^2 in this array corresponds to the light curve at z' from the model set that most closely matches the redshift of the reference light curve at z. Perfect reconstruction results in $z = z'$. Chi-squared values spanning the entire 1001×1001 $\{z, z'\}$ space are generated by choosing reference light curves over the interval $0 < z < 1$ in increments of 0.001. The $\chi^2(z)$ values reflects the degree of overlap between the light curve of a reference supernova located at redshift z with respect to the light curves of model supernovae located at z'. It bears emphasizing here that the reference and model sets are both drawn from the same Nugent template set. The overlap that would result if spectral variability were included undoubtedly would be less pronounced and the redshift reconstruction degraded from the present case. This degradation is studied further in Section 3.1.

3. RESULTS

Before considering complex template spectra it is instructive first to examine the χ^2 distribution of a simplified model. The

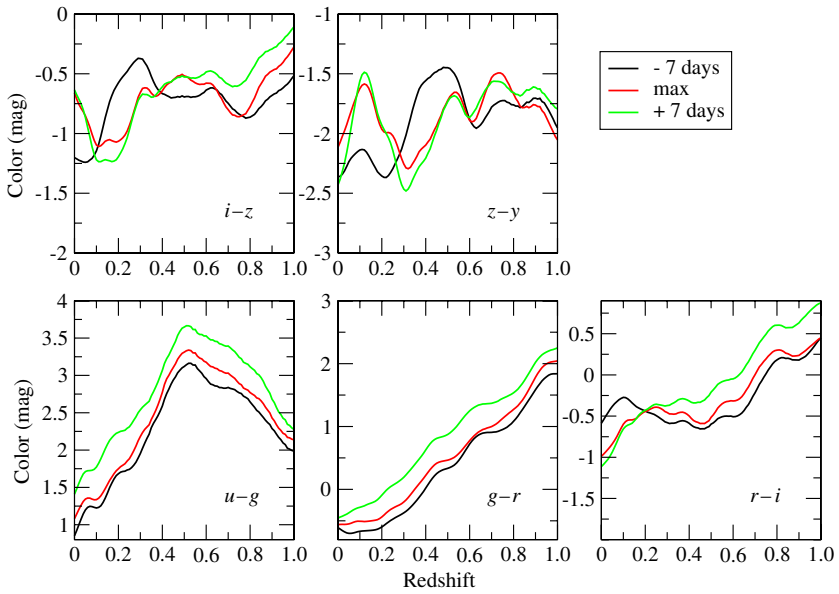

Figure 1. Lower left to upper right: $u-g$, $g-r$, $r-i$, $i-z$, and $z-y$ colors as a function of redshift at seven days before maximum (black), at maximum (red), and 7 days after maximum light (green) derived from the Nugent template and LSST filter sets.

(A color version of this figure is available in the online journal.)

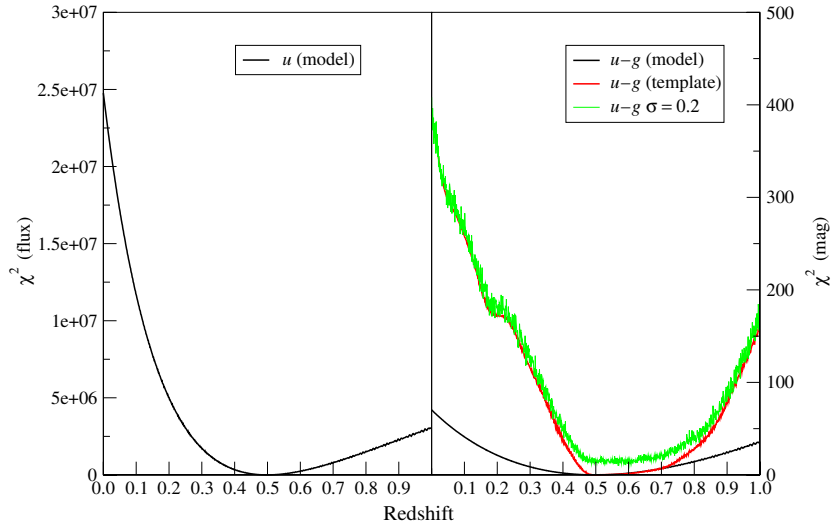

Figure 2. Left: χ^2 values (in units of flux) derived from the toy u bandpass and spectra described in the text. Right: χ^2 values for the $u-g$ color with no noise (red) and with the addition of noise drawn from a normal distribution with $\sigma = 0.05$ (green) using the Nugent templates and LSST $u-g$ color. For comparison purposes, results from the toy model derived from the $u-g$ color are also overlaid (black). All three curves in the right panel are computed in units of magnitudes. It is noteworthy that χ^2 curves derived from the Nugent template spectra are much steeper than that derived from the toy model—the temporal evolution of Type Ia supernova spectral features constrain possible redshift solutions.

(A color version of this figure is available in the online journal.)

curve in the left panel of Figure 2 represents the application of Equation (1) (but with $g(z) = g(z') = 0$) to a toy model where the rest-frame fluxes at all wavelengths and for all epochs are set to 1. These spectra are convolved with a toy u bandpass whose rest-frame transmission coefficients are also set to 1.0 over the wavelength interval 3190 Å $< \lambda <$ 4120 Å. This toy bandpass, in turn, is obtained by setting the transmission coefficients to 1.0 for each bin in the LSST u bandpass where the transmission coefficient exceeds 0.005, and zero elsewhere. More than 7 orders of magnitude differentiate the minimum at $z = 0.5$ from the maximum at $z = 0$ in this curve, suggesting considerable redshift discrimination with this approach. The black curve in the right hand panel of this same figure describes the χ^2 distribution for the $u-g$ color defined precisely by Equation (1), using the toy u bandpass described above in conjunction with a toy g bandpass whose rest-frame transmission coefficients are set to 1.0 over the region $3870 < \lambda < 5610$, and zero elsewhere. This second application of the toy model generates another featureless χ^2 distribution whose values are non-zero only because the u and g bandpasses possess different widths and are centered on different wavelengths. For the sake of comparison, this same panel also contains χ^2 values for the $u-g$ color derived from the Nugent templates and LSST bandpasses (red). Note that the χ^2 curve derived from the templates is much steeper than the toy model and, further, displays structure which can be traced back, in principle, to various spectral features.

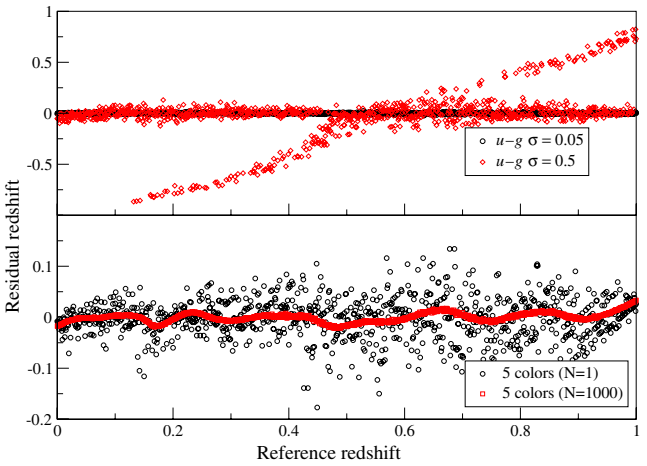

Figure 3. Top: residual redshifts as defined in the text for a single realization of noise drawn from a normal distribution with $\sigma = 0.05$ (black) and 0.5 (red) computed for the LSST $u - g$ color and assuming a nightly observing cadence. Bottom: same, but for a single realization (black) and the median of 1000 realizations (red) of noise drawn from normal distribution with $\sigma = 0.5$ using all five LSST colors.

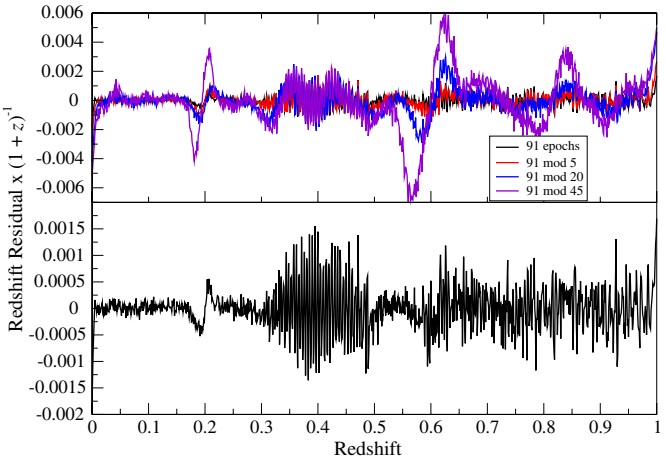

Figure 4. Bottom: median of the residual redshifts of 1000 realizations drawn from a normal distribution with $\sigma = 0.05$ for all five LSST colors and assuming a nightly observing cadence. Top: same, but assuming an observing cadence of every 5th night (red), 20th night (green), and 45th night (purple). For reference, the curve from the bottom panel is also included (black).

In the absence of noise, the reconstructed redshifts (corresponding to the minimum of the χ^2 distribution) in the examples above coincide with the chosen reference redshift of 0.5. A more realistic example includes measurement noise. The green curve in the right panel of Figure 2 represents the χ^2 values for the $u-g$ color also derived from the templates, but now where noise drawn from a normal distribution with standard deviation of 0.05 has been added to both the reference and model light curves. As this curve illustrates, the bin-to-bin jitter effectively broadens the minimum, increasing the likelihood that the location of the true minimum (located at z') will differ from the reconstructed minimum (located at z). For this particular realization of Gaussian noise the minimum of the χ^2 distribution is no longer $z = 0.5$, but $z = 0.569$, though the χ^2 values corresponding to these two redshifts are quite similar, i.e., 13.62 and 9.96, respectively.

To get a statistical measure of the effect that noise has on obscuring the location of the true minimum, Monte Carlo simulations consisting of 1000 random instances of photometric measurement noise were performed for each redshift interval. From each of the 1001 redshift bins, the median redshift from these 1000 simulations was compared to the redshift of the reference light curve. The top panel in Figure 3 are results from these simulations, each a plot of the residual redshift versus the redshift of the reference light curve using the LSST $u-g$ color as expressed by Equation (1). The residual redshift is defined here as $(z_{\rm rec} - z)/z$, where $z_{\rm rec}$ is the reconstructed redshift based on the above procedure and z is the redshift of the reference light curve. The sole difference between the curves in the upper panel of Figure 3 is the amount of Gaussian noise added to the reference and model light curves. It is seen that redshift reconstruction is quite faithful for the addition of Gaussian noise sampled from a normal distribution with a σ of 0.05, but erratic behavior is observed with a σ of 0.5. The bifurcation one observes in this panel for large photometric errors can be traced back to the non-monotonic nature of color versus redshift curve in Figure 1 ($u-g$ panel). Since for $z > 0.2$ (depending slightly on epoch) the $u-g$ color function is double-valued, for large σ the χ^2 minimization procedure alternates between two possible redshift solutions, giving rise to the aberrant behavior of the red curve in the upper panel of Figure 3. By this same logic, from Figure 1 one can predict more rational behavior for z in the vicinity 0.5, which is in fact manifestly observed in the residual redshift plot. As the lower panel of this same figure demonstrates, the erratic behavior in the top panel can be controlled when using all five color combinations of the LSST filter set. Though considerable bin-to-bin scatter is observed in the reconstructed redshift from only a single realization of Gaussian noise (black), 1000 realizations generate the smoothly varying curve (red) in this same panel. As noted above, the observed undulations ultimately can be traced to template spectral features passing through the bandpass filters. It is somewhat unexpected that a σ of 0.5 (corresponding to an S/N $\sim$ 2) generates no catastrophic outliers. Apparently, a nightly observing cadence could produce useful results even in the presence of considerable noise.

3.1. Light Curve Sampling

We next consider the effect of epoch sampling on redshift determination. The lower panel in Figure 4 shows the residual redshifts using all five bandpass colors applied to every epoch, but now with Gaussian noise drawn from a normal distribution with a σ of 0.05. In this plot, the residual redshifts are divided by a factor of $(1 + z)$. For this highly idealized cadence, the standard deviation of the redshift residuals is 4.2×10^{-4} over the redshift interval $0 \leqslant z \leqslant 1.0$. As it is clearly unrealistic for a survey instrument to sample any given supernova on a nightly basis, the upper panel in this same figure illustrates the impact of successively sparser sampling intervals on the residual redshifts. As a benchmark, the black curve from the lower panel is included, along with the residuals for cadences representing observations using all six LSST filters every 5th (red), 20th (green), and 45th (blue) night. The corresponding standard deviations are 5.2×10^{-4}, 9.2×10^{-4}, and 1.8×10^{-3}, respectively. Clearly, there are redshift intervals over which even an extremely sparse cadence may provide an accurate photometric redshift estimate. In any case, the data can be corrected for the bias (departure from perfect reconstruction) seen in these figures. By contrast, *errors* associated with the redshift residuals cannot be compensated for. Figure 5 is a

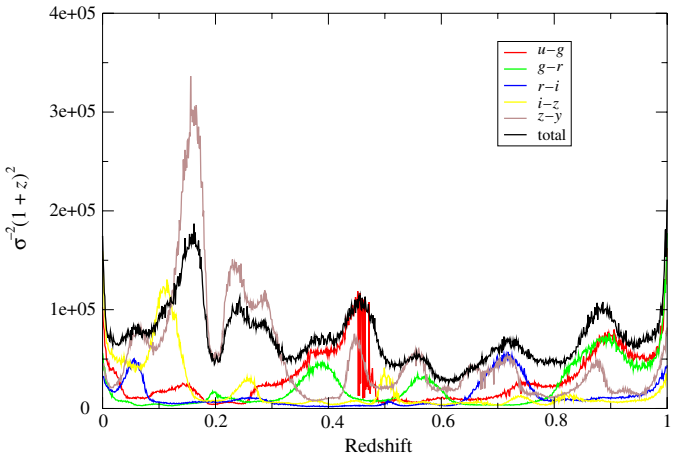

Figure 5. Inverse square of the errors of the redshift residuals from 1000 realizations of noise drawn from a normal distribution with $\sigma = 0.05$ and assuming an observing cadence of every 5th night in each of the five LSST colors, and the total inverse square error (black).

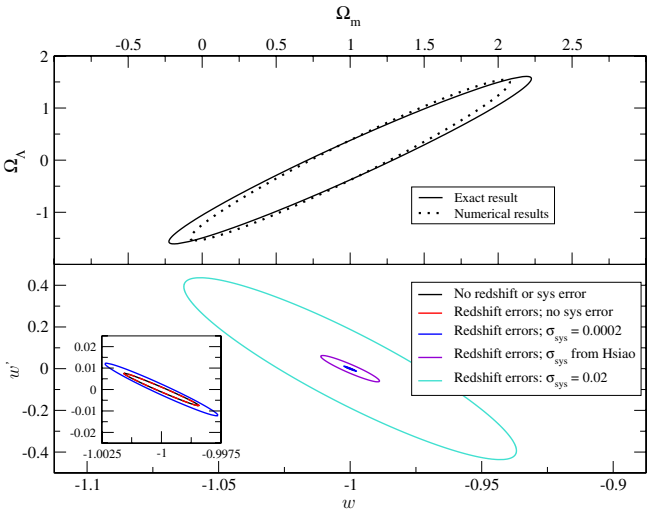

Figure 6. Top: error ellipses in the $\{\Omega_M,\Omega_\Lambda\}$ plane derived from analytical (solid) and discrete (dashed) implementations of the Gaussian supernovae distribution described in the text. In both cases, a flat, matter-filled universe ($\Omega_M = 1$, $\Omega_\Lambda = 0$) was assumed. Bottom: a series of five error ellipses in the $\{w, w'\}$ plane for various combinations of photometry, photometric redshift, and systematic errors as described in the text. A standard ($\Omega_M = 0.3$, $\Omega_\Lambda = 0.7$) cosmology is assumed in generating these five ellipses.

plot of the inverse square of the residual redshift errors for each of the five LSST colors assuming an observing cadence of every fifth epoch. In this plot, larger values correspond to smaller errors and illustrate the "effectiveness" of each color for reconstructing an accurate redshift over a given redshift range. This same plot also shows the total errors when all five colors are used (black curve). Note that even though σ^{-2} is an additive quantity, the sum from each of the individual colors does not quite equal that from the combined five colors since the colors are not linearly independent. The effectiveness of the $z-y$ color is particularly striking. Specifically, a conceivable strategy could be to restrict photometry to the z and y filters over the redshift interval $0.15 < z < 0.3$ should the templates resemble actual supernovae spectra in these bandpasses. As an optimal supernova cadence for LSST has yet to be adopted, based on the results from Figures 4 and 5 subsequent analyses are premised on the assumption that a particular supernova will be visited in each of the six filters every fifth night.

In addition to statistical errors arising from Poisson noise and further degraded by imperfect sampling, there may be a plethora of systematic errors that will further degrade photometric redshift accuracy. One systematic error that is relevant here concerns choice of templates. To generate binned systematic errors, we chose a second model template set constructed by Hsiao et al. (2007). This set has identical spectral wavelength coverage as the Nugent set, but epoch coverage is extended to +85 days (for this purpose, epochs beyond day 70 are ignored). We derive systematic errors by again computing the standard deviation in the redshift residuals for 1000 trails sampling from a normal distribution with $\sigma = 0.05$ and an observing cadence of every fifth night, but now using this second model set. The binned standard deviations that result are taken to be systematic error due to incompleteness of the Nugent template set and will be combined with other sources of error to derive error ellipses in Section 4.

4. COSMOLOGICAL PARAMETERS

Photometry, photometric redshift, and systematic errors each degrades the accuracy with which one can determine cosmological parameters. A common approach for propagating errors from data, or estimating the impact of errors from future data sets, is via the Fisher matrix. The Fisher matrix is a statistic which combines data errors with model sensitivities and whose inverse is the covariance matrix. Several techniques have been proposed for propagating redshift error using the Fisher matrix formalism; here we employ the method advanced by Huterer et al. (2004). In their approach, an $N \times N$ Fisher matrix (representing N cosmological parameters) is expanded by M rows and columns representing the M supernovae whose redshift errors are to be marginalized over. The off-diagonal terms in these M rows and columns contain cross products of derivatives of the distance modulus μ with respect to redshift times the derivatives of the distance modulus with respect to Ω_M or Ω_Λ, e.g., $\partial\mu/\partial z \cdot \partial\mu/\partial\Omega_M$. The M diagonal terms contain inner products of the form $\partial\mu/\partial z \cdot \partial\mu/\partial z$ and all such $M \times M$ terms are evaluated at the (binned) supernova redshift and weighted by the binned errors. When constructing the quantity $\partial\mu/\partial z$, the definition of μ is expanded to include stretch (but not derivatives of the K-corrections as was required in Huterer et al. 2004 as we are working with magnitudes derived directly from spectra, not light curves). As a cross-check of the technique, the error ellipse from this discrete method was compared with that derived from an analytical Gaussian distribution proposed by Tegmark et al. (1998). The upper panel in Figure 6 compares the exact result with the binned approach for a Gaussian distribution of 100 supernovae at an average redshift of z of 0.55, with a standard deviation of 0.2 and with a magnitude error of 0.5 for a flat, matter-filled universe ($\Omega_M = 1$, $\Omega_\Lambda = 0$). The variation between the two approaches is ascribed to the discrete binning (16 bins) that all but disappears as the number of bins approaches 100 (at the expense of computational resources required to invert a 102×102 matrix).

4.1. SN Ia Cosmology with LSST

We now ask how well a survey instrument like LSST, whose design is driven by weak lensing requirements, competes in the arena of SN Ia cosmology in the presence of errors computed in the previous section. Though its primary cadence may not be optimal for detection and follow up of Type Ia supernovae, LSST is nevertheless expected to discover several million Type Ia

Table 1
The Relevant Curve, the Number of Supernovae N_{SNe}, Photometric Error σ_p, Redshift Error σ_{red}, and Systematic Error σ_{sys} Used in Generating the Error Ellipses from Figure 6 [a]

Panel Location in Figure 1	Curve	N_{SNe}	σ_p	σ_{red}	σ_{sys}	σ_{Ω_M}	σ_{Ω_Λ}	σ_w	$\sigma_{w'}$
Top panel	Dotted	100	0.5	0.2	0	1.07	1.49	...	...
	Solid	100	0.5	0.2	0	1.22	1.56	...	...
Bottom panel	Black	10.25×10^6	0.17	...	...	...	...	0.002	0.0076
	Red	10.25×10^6	0.17	5.2×10^{-4}	...	...	...	0.002	0.0076
	Blue	10.25×10^6	0.17	5.2×10^{-4}	2×10^{-4}	...	...	0.003	0.0127
	Purple	10.25×10^6	0.17	5.2×10^{-4}	3×10^{-3}	...	...	0.012	0.066
	Cyan	10.25×10^6	0.17	5.2×10^{-4}	1×10^{-2}	...	...	0.063	0.413

Note. [a] The last four columns are the errors in the respective cosmological quantities computed at a 68% confidence level.

supernovae in the course of its 10 year mission. This sheer number of supernovae will allow unprecedented examination of systematics related to reddening, host contamination, evolution, and other effects that interfere with a precise determination of the distance modulus. Lacking a formal supernova cadence for LSST, we adopt the estimated number of supernovae per steradian per unit redshift per year in the observer frame as derived by Zhan et al. (2008). To discritize this distribution, a 2×2 Fisher matrix representing the cosmological parameters w and w' was expanded to an 18×18 matrix to accommodate 16 equally spaced redshift bins spanning $0 < z < 1.6$ (weights for $z > 1.0$ were made large to effectively confine the analysis to the interval $0 < z < 1.0$). We chose to parameterize the variation in w as $w(z) = w + zw'$. These 16 redshift bins were populated by various combinations of photometry, photometric redshift, and systematic errors. As both photometry and photometric redshift errors are quasi-statistical, each is reduced by the number of supernovae in each redshift bin; systematic error is non-statistical and is not affected by the number of supernovae. The resultant 18×18 matrix was inverted and marginalized along the 16 rows and columns representing the binned errors. The resultant 2×2 inverse matrix was again inverted to generate the error ellipses in Figure 6 given the inputs from Table 1.

Pure photometry error ($\sigma_p = 0.17$) generates the black ellipse in the inset of Figure 6. Photometric redshift errors associated with the red curve from the upper panel in Figure 5 ($\sigma = 0.05$; every 5th epoch) added in quadrature with photometry errors produce a second ellipse (red) that is indistinguishable from the first. This behavior, also noted by Huterer et al. (2004), is due to the magnitude of the photometry error: the degeneracy between the black and red ellipses would be lifted with more stringent photometry requirements. Various levels of systematic error are next added in quadrature to the photometry and photometric redshift errors. The blue ellipse in the inset arises from combined photometry, photometric redshift, and a small amount of systematic error added in quadrature. *Small* in this context refers to the scale of the systematic error with respect to other errors: the near-degeneracy of the blue ellipse with the black and red ellipses implies that the scale of chosen systematic error ($\sigma_{sys} \sim 0.0002$) is of the order of the photometry error divided by the square root of the number of supernovae per bin. Indeed, when adding in quadrature more substantial systematic error, such as that derived from the Hsiao template set ($\sigma_{sys} \sim 0.003$), the degeneracy is lifted. The largest ellipse (aquamarine) reflects the addition in quadrature of considerable systematic error (σ_{sys} of 0.02) in keeping with assumptions made by Huterer et al. (2004) and Zhan et al. (2008). Again, the term *considerable* acquires specific meaning in this context with respect to the magnitude of the photometry and photometric redshift errors.

5. DISCUSSION

A new era of large aperture ground-based survey telescopes is driving the need for an alternative to costly spectroscopic follow up to obtain Type Ia supernovae redshifts. In this paper, we apply a technique that utilizes templates to derive these redshifts photometrically based on a χ^2 minimization procedure. Though applied to proposed LSST bandpasses, this approach is broadly applicable to any instrument acquiring photometric data. Limited Poisson statistics, observational and instrumental noise, are modeled by the addition of Gaussian noise. Further, we approximate a realistic supernova campaign cadence by restricting the number of epochs used to construct our χ^2 figure of merit whose minimum is assigned to the redshift of the reference supernova. Multiple realizations of these simulations generate the statistics from which we extract the residuals and their standard deviations for each redshift bin. Ultimately, of course, we are interested in the implications for cosmology with redshifts derived in this manner. To proceed, we overlay a realistic redshift distribution broken into observing bins. Redshift errors are then placed in a matrix along with the weights of the cosmological parameters of interest, with a common multiplier reflecting photometry errors. Both the redshift errors and photometry errors are weighted by the number of supernovae per bin; binned systematic errors derived from a distinct model set are added in quadrature but are not weighted by the number of supernovae per bin. The resulting Fisher matrix generates error ellipses in the Ω_Λ and Ω_M and w and w' planes.

Though considerable work has been done to ascertain the feasibility of weak-lensing measurements from ground-based instruments (Wittman 2005; Jain et al. 2006; Asztalos et al. 2007), comparatively little has been done regarding Type Ia supernovae. This work is the first to put all the major elements together to ascertain the relevance of supernova cosmology from ground-based instruments. In particular, it establishes a minimal redshift error that can be expected from photometric redshift determination. The purple error ellipse in Figure 6 derived from plausible photometric redshift and systematic errors is considerably more constrained than would be the case if one assumed constant photometric redshift and systematic errors ~0.02 that have appeared in the literature (Huterer et al. 2004; Zhan et al. 2008). A corollary is that should

systematic error ultimately be controllable to ∼0.003, then photometric redshifts should be effective at discriminating among competing cosmologies. A more realistic observing cadence, Type Ia supernova distribution, and noise models are readily incorporated into this framework. Indeed, though the scope of this work has been strictly limited to template models, it is readily modified to actual supernova spectra. Progress is being made toward extending this work to include simulated cadences and actual Type Ia supernova spectra and work continues on improved noise models. Extensions of this work must further address covariances among the techniques used for typing, epoch, and redshift assignments.

We conclude with a final observation. At present, this method is limited to stretch ∼1 supernovae since, at present, there is no firm consensus as to the underlying mechanism for stretch. However, correlations between various spectral features and stretch are well established (Nugent et al. 1995; Wagers et al. 2010), and with these correlations in hand we have embarked on the construction of Type Ia supernova templates with stretch different from one. With these templates in hand, the above technique could be extended by an additional loop over templates representing varying degrees of stretch. One advantage to templates constructed in this manner is that the variability would not necessarily be restricted to that observed in actual Type Ia supernovae (Guy et al. 2007).

We acknowledge Dragan Huterer for help in implementing his Fisher matrix analysis.

REFERENCES

Astier, P., et al. 2006, A&A, 447, 31
Asztalos, S., de Vries, W. H., Rosenberg, L. J., Treadway, T., Burke, D., Claver, C., Saha, A., & Puxley, P. 2007, ApJ, 659, 69
Bolzonella, M., & Pelló, R. 2000, in ASP Conf. Ser. 200, Clustering at High Redshift, ed. A. Mazure, O. Le Fèvre, & V. Le Brun (San Francisco, CA: ASP), 392
Connolly, A. J., Csabai, I., Szalay, A. S., Koo, D. C., Kron, R. G., & Munn, J. A. 1995, AJ, 110, 2655
Goldhaber, G., et al. 1996, Nucl. Phys. B Proc. Supp., 51, 123
Guy, J., et al. 2007, A&A, 466, 11
Hillebrandt, W., & Niemeyer, J. C. 2000, ARA&A, 38, 191
Hsiao, E. Y., Conley, A., Howell, D. A., Sullivan, M., Pritchet, C. J., Carlberg, R. G., Nugent, P. E., & Phillips, M. M. 2007, ApJ, 663, 1187
Huterer, D., Kim, A., Krauss, L. M., & Broderick, T. 2004, ApJ, 615, 595
Jain, B., Jarvis, M., & Bernstein, G. 2006, J. Cosmol. Part. Phys., JCAP02(2006)001
Loh, E. D., & Spillar, E. J. 1986, ApJ, 303, 154
Nugent, P., Kim, A., & Perlmutter, S. 2002, PASP, 114, 803
Nugent, P., Phillips, M., Baron, E., Branch, D., & Hauschildt, P. 1995, ApJ, 455, L147
Olivier, S. S., Seppala, L., & Gilmore, K. 2008, Proc. SPIE, 7018, 70182
Perlmutter, S., et al. 1999, ApJ, 517, 565
Riess, A. G., et al. 1998, AJ, 116, 1009
Tegmark, M., Eisenstein, D. J., & Hu, W. 1998, arXiv:astro-ph/9804168
Wagers, A., Wang, L., & Asztalos, S. 2010, ApJ, 711, 711
Wang, Y. 2007, ApJ, 654, L123
Wang, Y., Narayan, G., & Wood-Vasey, M. 2007, MNRAS, 382, 377
Weinberg, S. 1972, Gravitation and Cosmology: Principles and Applications of the General Theory of Relativity (Weinheim: Wiley-VCH)
Wittman, D. 2005, ApJ, 632, L5
Wood-Vasey, W. M., et al. 2007, ApJ, 666, 694
Zhan, H., Wang, L., Pinto, P., & Tyson, J. A. 2008, ApJ, 675, L1